Design and Electromagnetic Analysis of a New Rotary-Linear Switched Reluctance Motor in Static Mode

M. M. Nezamabadi, E. Afjei, and H. Torkaman

Faculty of Electrical Engineering
Shahid Beheshti University, G.C., Tehran, Iran
{m_nezamabadi, e-afjei, h_torkaman}@sbu.ac.ir

Abstract ─ A newly designed rotary-linear switched reluctance (RLSRM) motor is presented and electromagnetically analyzed in this paper. The motor has an integrated structure and can control both linear and rotary motions. It is mainly designed to control the engagement of a rotating gear. For this purpose a two-section motor comprised of a rotary and a linear SRM is designed. In the middle part of the motor assembly, a three-phase rotary SRM with 6 stator and 4 rotor poles creates rotary motion. The linear section which is a transverse flux two-phase SRM is composed of two parts placing at each side of the rotary section. The cylindrical translators inside the linear stator poles provide short magnetic flux paths which reduce the core losses and increase the force per volume. The motor parameters derived from the motor design procedure are evaluated using 3-dimensional finite element analysis (3DFEA). The motor performance indices such as flux linkages, flux density, mutual flux, static torque and force for various loads are obtained and assessed for rotary and linear motions. Finally, a comparative study is performed and 3DFEA results are compared with two different RLSRM structures. The comparison shows that the proposed structure has the highest force per motor volume.

Index Terms ─ Electromagnetic analysis, finite element analysis, rotary-linear motion, switched reluctance motor.

I. INTRODUCTION

Switched reluctance motors have become a popular alternative for variable speed drives in recent decade. Simple structure, lack of magnetic material or coil on the moving part, fault tolerance, and low manufacturing and maintenance costs have changed it to a serious competitor for induction and brushless DC motors [1-5]. In contrast with many of the DC and AC motors, SRMs need a control system for normal operation. This requirement restricted its utilization but appearing low cost power semiconductors accelerated its application in recent years. Rotary and linear structures have been developed for SRMs with a variety of applications. For rotary type, different variable speed applications such as home appliances, electric and hybrid electric vehicles have been introduced. Linear SRM has been used in elevators and electrical trains [6-9].

Rotary and linear motions are needed together in several applications. Power transmission systems in automatic or electrical vehicles, robots, wire winding machines, weaving equipment, and component insertion systems are among the known applications [10]. Usually, two or more motors or combination of pneumatic, hydraulic, and electric systems are needed to provide the motions required in these applications. Conventional systems for rotary-linear motion control are often accompanied by some mechanical parts such as gears or belts. These systems require frequent maintenance and adjustment that decrease the whole system reliability [11]. Less mechanically complicated and more electronically controllable solutions for rotary-linear motion control are highly demanded. Rotary-linear electrical motors providing both rotary and linear motions in an integrated structure are a good alternative for conventional electro-hydraulic systems [12]. These rather newly appeared motors can bring more controllability and precision, faster response and higher efficiency with less cost and space [13].

Several structures for rotary-linear motors based on SRM technology have been reported in the literature in recent years [14-19]. In [14], a RLSRM consisting of two separate stators and a rotor-translator is proposed. The rotary and linear motions are controlled by the optical sensors inside the motor and the linear position sensor mechanically coupled to the shaft, respectively. The motor operation depends on the precision and adjustment of two sensor types which impose cost and complexity to the system and reduce the reliability. For this structure, a control strategy based on the multiphase excitation method has been reported in [15,16]. A torque and force distribution function is proposed for the RLSRM to decouple the two axes of motion. The control strategy is still dependent to the sensors information.

Another RLSRM with two different structures for rotary and linear stators is introduced in [17]. Due to the

Submitted On: July 20, 2015
Accepted On: December 5, 2015

encoder coupling to the motor, the shaft is only accessible from one side. The long rotor creates magnetic interference for rotary and linear motion control.

Two different RLSRM structures with their electromagnetic simulations are exposed in [18,19]. Using position sensors and the interference of rotary and linear motions control have increased the complexity in all of the proposed RLSRMs.

In the structures that utilize multi-stacks of slotted rotor [14-18], excitation of the linear phases produce torque and the motor has combined rotary-linear motion instead of pure linear motion. So at least they need a decoupling strategy to decouple rotary and linear motion control [15,16]. In multi-stack RLSRMs the number of rotor poles are less than the number of stator poles. So it is not possible to utilize all of the rotor and stator cores capacity for linear force production as only one stator phase poles are in rotationally aligned position at each time and can be used for linear motion without torque production.

The main purpose of this paper is proposing a new RLSRM for independent control of the rotary and linear motions. The completely separated magnetic flux paths decouple the motor operation in rotary and linear modes and give the possibility to control two-axis motion both simultaneously and separately.

In this research, the new RLSRM is capable of working in three different modes: 1- Rotary, 2- Linear, 3- Rotary-linear (RL). For solving the problems originated from slotted translators, two cylindrical translators have been used. Also, the hybrid motion control by the constructed RLSRM does not need any decoupling control algorithm, which is an important issue in the other rotary-linear motors. The decoupled rotary and linear motion control and simple integrated structure are the advantages of the proposed RLSRM.

In the following, after a discussion about the design procedure of the motor in Section 2, the design verification by 3DFEA is presented in Section 3. For design verification, static analysis is performed by 3DFEM. Based on the available information for the other RLSRMs structures, a comparative study has been performed at the end of Section 3. Finally, the consequences of this research are described in Section 4.

II. DESIGN AND THEORETICAL ANALYSIS OF THE NEW RLSRM

The motor is designed to engage and disengage a rotating gear in a wire winding machine. It is comprised of two sections, each one responsible for one axis motion control. The rotary section which is a radial field rotary SRM is in the middle part of the motor assembly. It has 6 salient poles on the stator and 4 on the rotor. The coils on the stator opposite poles are serially connected and form a phase. Therefore, the motor has 3 phases that should be excited sequentially to rotate the rotor. Since the motor shaft has both rotary and linear motions, the rotor stack length has been considered as the half of the stator stack length. The linear section is a two phase transverse flux LSRM with active stators and passive translators. Each phase is comprised of a six-pole stator and a cylindrical translator situated at both sides of the rotary section. For the sake of simplicity, the linear and rotary stators have the same structures. The structure of the new RLSRM is illustrated in Fig. 1.

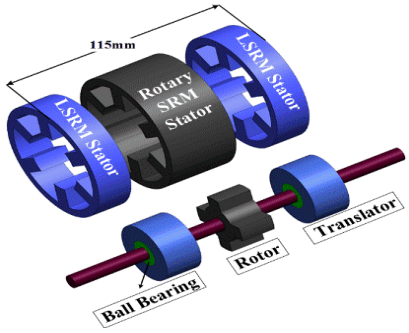

Fig. 1. The proposed structure for RLSRM.

All of the coils in each linear stator phase are serially connected and excited together. The coils are wrapped around the poles in a way that make opposite magnetic poles in two neighbor stator poles. Therefore by exciting a phase coils the magnetic flux finds short paths inside the translator. The short magnetic flux paths increase the motor efficiency by reducing the magnetic core losses. During a phase excitation 6 magnetic circuits are established by the translator, stator pole windings, and two air gaps. The translator moves toward more overlap with the stator poles in order to create the magnetic circuit with minimum reluctance. The configuration of the linear section facing the front view is depicted in Fig. 2.

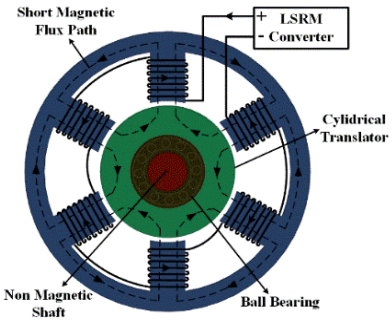

Fig. 2. The front view of the linear section.

If the translator rotates while the linear phase coils are energized, the magnetic field induced in the translator produces undesirable negative torque. Therefore, each translator is coupled to the shaft by a pair of ball bearings. The bearings are fixed on the shaft so that the

coupled translator can rotate freely while it cannot move linearly relative to the shaft. In this way, the translators can have linear motion while the shaft is rotating inside the bearings. For retaining the shaft so that it can move linearly while rotating, one slide-rotary bush (SRB) couples the shaft to the motor cap at each side. The structure of the SRB is shown in Fig. 3.

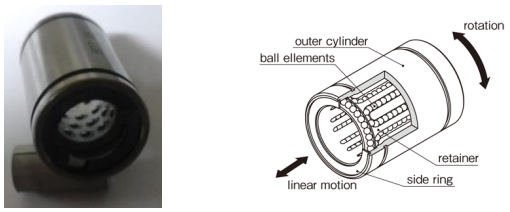

(a) (b)

Fig. 3. (a) The used slide-rotary bush, and (b) the internal structure of the slide-rotary bush [20].

The SRBs retain the shaft at the center of rotation axis while the shaft can rotate and slide freely on the SRB ball elements.

A. Design procedure-rotary section

For decoupling the control of rotary and linear motions, separate structures are considered for each kind of motion. The motor design starts with selecting parameters for a radial field 3-phase, 6/4 rotary SRM. The output equation of a SRM is given by:

$$P_o = K_m B A_s D^2 L N, \quad (1)$$

in which P_o is the output power, A_s is the specific electric loading, D is the bore diameter, and N is the rotor speed in RPM. K_m is a factor depends on several parameters such as the motor efficiency, duty cycle, and saturated and unsaturated inductances [3]:

$$D = \sqrt[3]{\frac{P_o}{K_m k B A_s N}}. \quad (2)$$

The rotor stack length is calculated by:

$$L = kD, \quad (3)$$

in which k is a parameter that depends on the nature of the application. The range of k for non-servo applications is:

$$0.25 < k < 0.7. \quad (4)$$

Assuming β_s and β_r as the stator and rotor pole arcs, the width of stator and rotor poles t_s and t_r can be calculated as:

$$t_s = D \sin\left(\frac{\beta_s}{2}\right), \quad (5)$$

$$t_r = D \sin\left(\frac{\beta_r}{2}\right). \quad (6)$$

The range of stator and rotor yoke thicknesses, S_y and R_y are given by:

$$0.5t_s < S_y < t_s, \quad (7)$$

$$0.5t_r < R_y < 0.75t_r. \quad (8)$$

The magnetic field intensity in the air gap is obtained from (9):

$$H_g = \frac{B}{\mu_0}. \quad (9)$$

The number of turns per phase for a peak current of I_p is:

$$N_{ph} = \frac{H_g \times 2g}{I_p}. \quad (10)$$

The cross section of the conductor is calculated from (11) in which J is the conductor current density:

$$A_c = \frac{I_p}{J\sqrt{q}}. \quad (11)$$

For obtaining the stator pole height, h_s it is required to calculate the stator coil width, C_w and height C_h. Subtracting the stator pole arc lengths and the distances between adjacent coils from the bore periphery, the coil width can be calculated from (12):

$$C_w = \frac{\pi D - P_s\left[\beta_s \cdot \frac{D}{2} + C_g\right]}{2P_s}, \quad (12)$$

in which P_s is the number of stator poles and C_g is the gap between the stator adjacent coils. The stator coil height is achieved from (13):

$$C_h = \frac{a_c N_{ph}}{2C_w}. \quad (13)$$

The stator pole height is specified considering the span given in (14):

$$C_h < h_s < 1.4C_h. \quad (14)$$

The rotor pole height, h_r is obtained by applying the calculated parameters in the previous steps to (15):

$$h_r = \frac{D - 2(g + R_{sh} + R_y)}{2}, \quad (15)$$

in which R_{sh} is the shaft radius.

Table 1 shows the final parameters of the rotary SRM obtained from theoretical formulation.

Table 1: Specifications of rotary SRM

Parameter	Value	Parameter	Value
Rated power	80 W	Rotor pole width	10 mm
Rated speed	3000 RPM	Stator pole width	8.8 mm
Air gap	0.25 mm	Rotor yoke thickness	5.4 mm
Supply voltage	48 V	Stator yoke thickness	5 mm
Phase peak current	2.5 A	No. of turns/coil	120
No. of stator poles	6	Rotor stack length	17.5 mm
No. of rotor poles	4	Stator stack length	35 mm
Specific elec. loading	28500 A/m	Rotor pole height	7.3 mm
Rotor pole arc	32 Deg.	Stator Pole height	13 mm
Stator pole arc	28 Deg.	Rotor pole width	9.8 mm
Shaft radius	5 mm	Stator pole width	8.7 mm
Current density	5 A/m^2	Bore diameter	36 mm
k	0.48	Conductor cross section	0.3 mm^2

B. Design procedure-linear section

For controlling the engagement of a rotating gear a

two-phase transverse flux LSRM is designed to create forward-backward movement. Before designing the LSRM several assumptions should be considered. The required linear force and displacement are 14 N and 17.5 mm, respectively. For having simple and uniform structure the linear stator is considered the same as the rotary stator with less stack length. The motor structure side view is illustrated in Fig. 4.

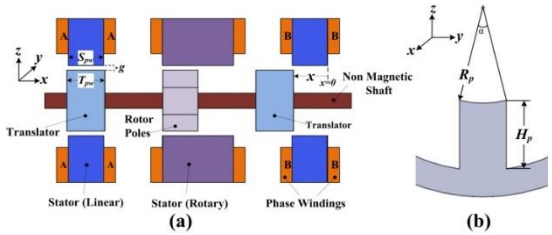

Fig. 4. (a) The structure of the RLSRM facing the side view, and (b) the linear stator structure.

Considering a linear phase, the variation of magnetic energy in the air gap as a result of translator movement can be calculated by:

$$dW_f = \frac{1}{2} B_{ag} H \; dV, \tag{16}$$

in which B_{ag} is the magnetic flux density in the air gap, H is the magnetic field intensity and dV is the air gap volume variation. The air gap volume variation as a result of translator movement along the x-axis will be:

$$dV = dA_{tp}\, g = R_p\, \alpha \left(S_{pw} - x\right) g, \tag{17}$$

where A_{tp} is the overlapping area of the translator and one stator pole, g is the air gap, R_p is the bore radius, α is the stator pole angle, x is the axial translator displacement, and S_{pw} is the stator pole width. The linear force, f_L for a constant exciting current can be calculated as:

$$f_L = \frac{\partial W_f}{\partial x} = \frac{1}{2} \frac{B_{ag}^{\;2}}{\mu_0} \left(-R_p \alpha\right) g. \tag{18}$$

By neglecting the translator and stator core reluctances against the air gap reluctance the magneto motive force (mmf) is achieved:

$$\Im \cong \frac{B_{ag}}{\mu_0} g. \tag{19}$$

Considering (17) and (18) reveals that the force is only a function of mmf, stator pole circumferential length ($R_p\alpha$) and air gap:

$$f_L = -\frac{1}{2} \mu_0 \Im^2 \frac{R_p \alpha}{g}. \tag{20}$$

By utilizing variable equivalent air gap permeance model for SRM [21], it is possible to develop an equation for the linear force produced by one phase excitation:

$$f = \frac{6}{\mu_0} \frac{P_c}{K_c K_s} B_{ag}^{\;2} . g . \alpha . R_p, \tag{21}$$

in which K_c is Carter's factor and P_c is the permeance coefficient. K_s is saturation coefficient depended to the core material magnetic characteristics and the length of magnetic flux path in the core and air gap. The required slot area A_w for winding as a function of air gap flux density B_{ag}, current density J, and fill factor K_w is obtained:

$$A_w = \frac{2g\, B_{ag}}{\mu_0 J\, K_w}. \tag{22}$$

For designing the linear section the following parameters are considered initially: air gap length g, air gap flux density B_{ag}, stator slot fill factor K_w, saturation coefficient K_c, Carter's coefficient K_s, permeance coefficient P_c, and current density J. The winding area obtained from (23). Applying (19), the required mmf per coil is achieved. So for the peak current value the number of turns per coil can be calculated. The required 14 N linear force gives the stator pole circumferential length from (20) $R_p.\alpha$. Since the rotary and linear stator structures are the same, the optimized R_p and α are calculated, respectively. The prior assumptions and the calculated parameters for the linear section are summarized in Table 2.

Table 2: Specifications of the linear SRM

Parameter	Value	Parameter	Value
Air gap	0.25 mm	Peak current	4 A
B_{ag}	1.6 T	Slot area (A_w)	3 cm^2
Slot fill factor	0.4	mmf/coil ($\Im$)	300 A.t
Saturation coeff.	1.6	No. of turns/coil	75
Carter's coeff.	1.4	Bore radius	18 mm
Permeance coeff.	1.3	Stator pole arc	28 Deg.
Current density	5×10^6 A/m^2		

Considering the motor whole volume V, the motor force per volume, F_v is:

$$F_v = \frac{F_{lmax}}{Motor\,Volume} = \frac{14}{\pi \times (40)^2 \times 140 \times 10^{-9}} = 19894 \left[N/m^3 \right]. \tag{23}$$

For design verification, the proposed structure completely analyzed with 3DFEM and the results are given in the following section.

III. ELECTROMAGNETIC ANALYSIS OF RLSRM USING 3DFEM

Complete and accurate modeling of the designed motor is a necessary step in verifying the obtained parameters from analytical calculations. Finite element method is a precise and efficient solution for modeling and analyzing magnetic circuits. Although it is more complex and time consuming, 3DFEA of the machine has remarkable advantages over 2D. Some practical parameters such as the motor length effects cannot be

considered in 2D analysis. For starting the analysis geometric and magnetic model of the motor are specified then the boundary conditions and polynomial order are set. Based on the input information, the initial 3D meshing is performed and the magnetic field distribution is calculated inside and around the motor layout. Based on the achieved magnetic field distribution, some other parameters such as flux linkage, core losses, and torque (force) can also be obtained. Figure 5 shows the initial 3D mesh layout of the designed RLSRM in Magnet CAD package for analysis [22].

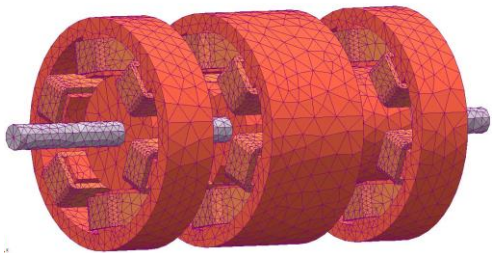

Fig. 5. 3D finite element meshing of the designed RLSRM.

Both stator and rotor cores are made up of non-oriented silicon steel laminations, while the shaft is from non-magnetic material. Static analysis is performed by 3DFEM and the results are given in the following.

A. Static electromagnetic analysis of RLSRM

For static analysis after determining the geometric model, the parameters of 3DFEA are set. For the rotary SRM, the coils of one phase are energized and the magnetic field distribution is calculated from unaligned to the next unaligned positions.

Fig. 6Figure 6 illustrates the magnetic flux density and flux path with the motor poles in unaligned and aligned positions. The coils of phase A are energized with 2A constant current and the rotor rotates with mechanical resolution of 0.5 degree. In each step, the magnetic field distribution is calculated and recorded. The flux density of the rotor pole is about 0.97 and 0.1 Tesla for aligned and unaligned positions.

The variation of flux linkage with refer to the rotor pole position is shown in Fig. 7, for various excitations. Regarding to four times excitation of phase A in one rotation, its flux linkages are raised according to the rotor position. As shown in this figure, the maximum amplitude of flux linkage is about 33, 25, 17 and 8 mWb at aligned rotor position for 2, 1.5, 1 and 0.5 A, respectively.

The angular position is measured between the center of two adjacent rotor poles and the center of the excited stator pole. By starting the rotor and stator poles overlap the magnetic circuit would have the maximum inductance variation versus rotor position. In Fig. 7, the rotor and stator poles overlap starts at 15°. Since the rotor can move linearly inside the stator, the analysis of the flux linkage is performed in 3 different linear positions with 1 A excitation current. The results of the analysis with the rotor at the sides and middle of the stator are exposed in Fig. 8.

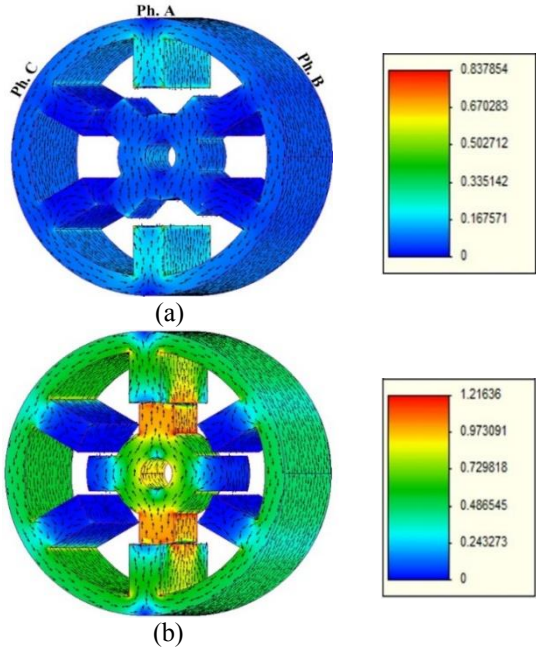

Fig. 6. Flux density and flux path of the rotary section at: (a) unaligned, and (b) aligned positions.

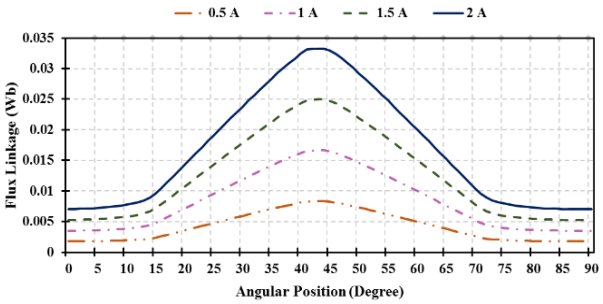

Fig. 7. Variation of flux linkage versus the rotor pole angular position in rotary motion mode.

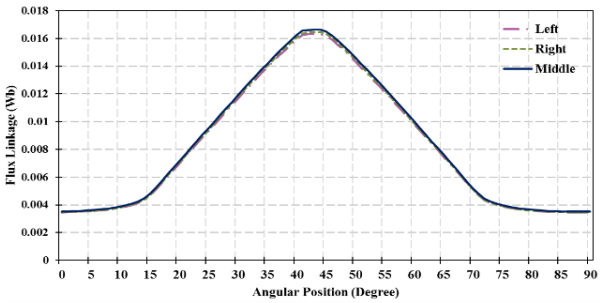

Fig. 8. The effect of the rotor linear motion on flux linkage.

Figure 8 reveals that the linear movement of the rotor does not have considerable effect on the rotary SRM performance.

The amount of magnetic flux that closes its path from two idle phases is considered as the mutual flux. This portion of the magnetic flux does not cooperate in torque production and should be as low as possible. Figure 9 shows the mutual flux of two idle phases as a result of a phase excitation.

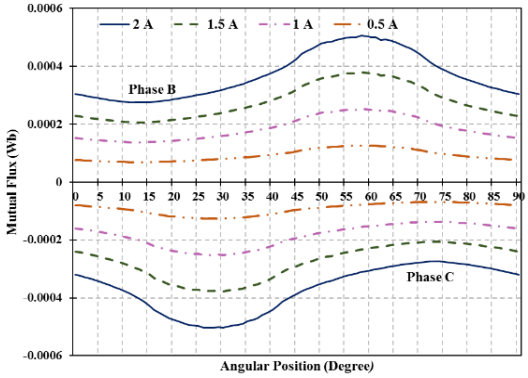

Fig. 9. Mutual flux of two idle phases in rotary motion mode.

The maximum leakage is about 0.5 mWb, which is 1.25% of the maximum flux linkage. This phenomenon helps to minimize the power losses.

The torque in a SRM can be obtained from:

$$T = \frac{\partial W'_f(i,\theta)}{\partial \theta}\Big|_{i=constant} \cong \frac{1}{2}\frac{dL(\theta,i)}{d\theta}\, i^2, \qquad (24)$$

where $W'_f(i,\theta)$ is the magnetic circuit co-energy, θ is the rotor pole angle, L and i are the phase inductance and current, respectively. The static torque as a result of 90° rotor rotation is depicted in Fig. 10. Based on Equation (24) as shown in Fig. 10, the static torque is raised when the excitation current goes up, in which the torque of the motor reaches to 0.25 N.m in the rated current.

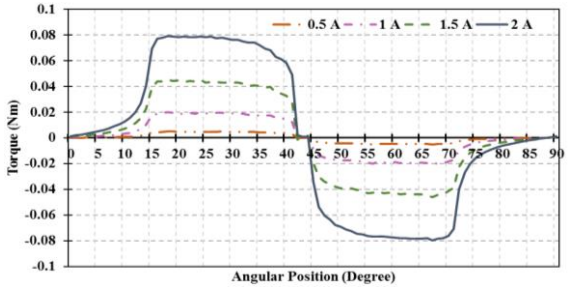

Fig. 10. The static torque from unaligned to the next unaligned position rotary motion mode.

The motor linear operation analysis is performed via 3DFEM while all of coils in one phase are energized. The magnetic field distribution is calculated from the translator unaligned to aligned positions. The magnetic flux path and the magnetic field distribution in stator and translator are depicted in Fig. 11 for linear motion mode. All of the stator windings are excited with 2 A current. The flux density of the translator is about 1 and 0.25 Tesla for aligned and unaligned positions. Each magnetic circuit comprised of two stator poles, two air gaps, translator, and stator back iron, which creates a short magnetic flux path in the translator. The analysis is performed with 0.5 mm step from unaligned up to full aligned position.

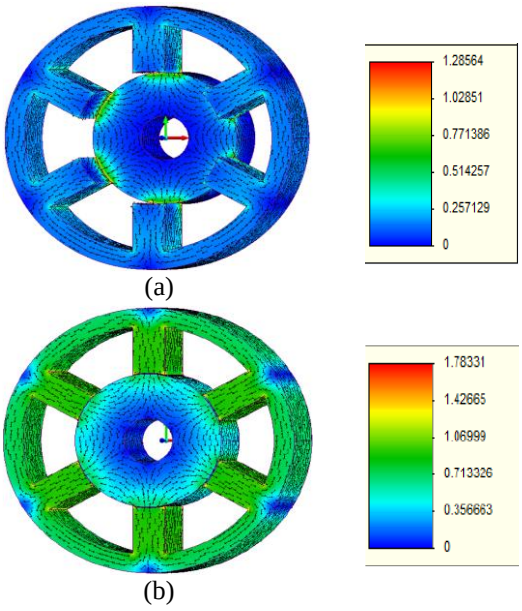

Fig. 11. Flux density and flux path of the motor in linear motion mode at: (a) unaligned, and (b) aligned positions.

The shape of flux linkage during one linear stroke is illustrated in Fig. 12. The flux linkage analysis has been performed for 4 different current values. As shown in Fig. 12, flux linkage of the coil in phase A has 13, 23, 32 and 37 mWb maximum amplitudes when the motor is excited with 1, 2, 3 and 4A, respectively, in the linear motion mode.

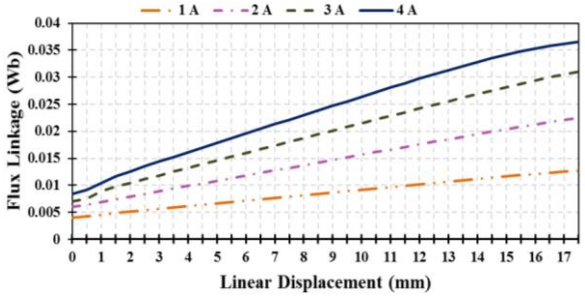

Fig. 12. Flux linkage of a phase during one stroke for linear motion mode.

Energizing the phase coils brings the translator to a position with less reluctance and hence more overlap with the stator. The position of the translator is measured between the edges of the stator pole and the translator.

Linear force is analyzed statically with the translator movement in 0.5 mm step. The analysis results for 4 different current magnitudes are given in Fig. 13. As shown in this figure, when the excitation current goes up from 1 A to 2, 3 and 4 A, the amplitude of produced motion force in RLSRM is increased by 4, 8.5, and 14 times higher.

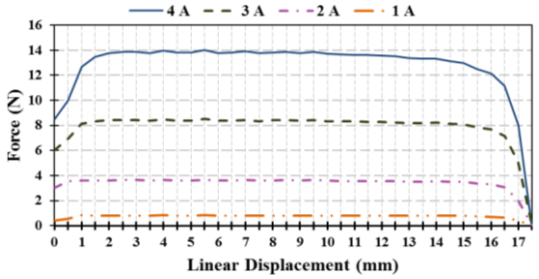

Fig. 13. The linear force for different excitation currents during one stroke.

The core losses decrease as a result of short flux paths in the translator. Energizing 6 stator coils together and the short magnetic flux paths increases the motor force per volume, which will be discussed in the next section.

B. Comparative study

After verification of the obtained parameters from the design procedure and FEM verification, a prototype is fabricated in the laboratory. Figure 14 shows the structure of different parts of the constructed motor.

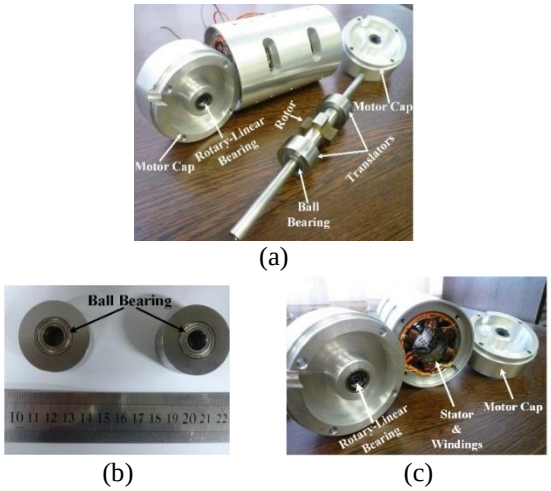

(a)

(b) (c)

Fig. 14. Constructed RLSRM structure: (a) motor parts, (b) translator structure, and (c) motor cap, stator and windings.

In order to show any improvement in the motor performance, it is required to compare the motor output parameters with the parameters of the similar structures. The motor parameters are compared with the parameters of two RLSRMs found in the literature. The RLSRMs presented in [14] and [16] are based on a same structure. They have two identical 6-pole stators and an extended 4-pole rotor. Based on the given information the following parameters can be extracted: 1- Force and torque per mmf per volume for the motor in [14], 2- Force and torque per mmf per mass for the motors in [16], [17]. Table 3 shows the parameters of the constructed RLSRM and the other comparable structures in the literature.

Table 3: Comparison of the motor parameters with other RLSRMs

Parameter	Proposed RLSRM	RLSRM [14]	RLSRM [16]	RLSRM [17]
Force per volume ($N/m^3.A.t$)	11.05	8.92	DNA*	DNA
Force permass ($N/kg.A.t$)	2.88×10^{-3}	DNA	2.53×10^{-3}	2.13×10^{-3}
Torque per volume ($N.m/m^3.A.t$)	0.59	0.44	DNA	DNA
Torque per mass ($N.m/kg.A.t$)	1.19×10^{-4}	DNA	1.33×10^{-4}	1.01×10^{-4}

*Data not available

The constructed motor has the highest linear force among the studied structures. The normalized force and torque per volume show 23% and 34% increase with reference to the motor in [14], respectively. The normalized force per mass is 14% more than its corresponding value in [16]. The normalized torque per mass is 11% less than the value of [16]. This reduction can be interpreted as the constructed motor does not utilize a considerable part of the motor volume for rotary motion. This can be considered as the main disadvantage of the proposed structure. It should be noted that this special structure decouples rotary and linear motion control. Although the rotary section does not have any contribution in linear motion, the short magnetic flux paths give the highest force to the constructed motor. Therefore, the motor operation in rotary, linear and rotary-linear modes is applicable with improved characteristics in comparison with the other ones. As shown experimentally, the compound rotary-linear motion control by the constructed RLSRM does not need any decoupling control algorithm which is an important issue in the other rotary-linear motors [15,16]. The decoupled rotary and linear motion control and simple integrated structure are the advantages of the proposed RLSRM that make it a good competent for the other rotary–linear motors.

IV. CONCLUSION

A new structure for rotary-linear motion control based on SRM technology has been presented. The parameters of the RLSRM are calculated from rotary and linear SRM design equations. Verification of the calculated values is performed by the model analysis via 3D-FEM. The static electromagnetic analysis of the motor gives the static torque, linkage and leakage fluxes and linear force. The achieved flux linkage was about 40 mWb with minimum leakage about 0.5 mWb, which proves the low motor loss. Also, the power of flux density was 0.97 and 1 Tesla in rotary and linear motion modes, respectively. A prototype has been fabricated based on the design parameters. The comparative study has been performed and shows that the motor has the highest force per volume among the studied RLSRM structures (i.e., the normalized force and torque per volume show 23% and 34% increase in comparison with other ones). These achieved results show the applicability of the proposed motor in different applications for rotary, linear and rotary-linear modes of operation.

REFERENCES

[1] L. Xiang, S. Zuo, L. He, M. Zhang, J. Hu, and G. Long, "Optimization of interior permanent magnet motor on electric vehicles to reduce vibration caused by the radial force," *Applied Computational Electromagnetics Society Journal*, vol. 29, 2014.

[2] E. Afjei, M. Tavakoli, and H. Torkaman, "Eccentricity compensation in switched reluctance machines via controlling winding turns/stator current: theory, modeling, and electromagnetic analysis," *Applied Computational Electromagnetics Society Journal*, vol. 28, 2013.

[3] R. Krishnan, *Switched Reluctance Motor Drives: Modeling, Simulation, Analysis, Design, and Applications*, CRC Press, 2010.

[4] H. Torkaman, N. Arbab, H. Karim, and E. Afjei, "Fundamental and magnetic force analysis of an external rotor switched reluctance motor," *Applied Computational Electromagnetics Society Journal*, vol. 26, 2011.

[5] E. Aycicek, N. Bekiroglu, I. Senol, and Y. Oner, "Rotor configuration for cogging torque minimization of the open-slot structured axial flux permanent magnet synchronous motors," *Applied Computational Electromagnetics Society Journal*, vol. 30, 2015.

[6] C. He, H. Chen, and Y. Zhou, "Design indicators and structure optimisation of switched reluctance machine for electric vehicles," *Electric Power Applications, IET*, vol. 9, pp. 319-331, 2015.

[7] J. Lin, K. W. E. Cheng, X. Xue, N. C. Cheung, and Z. Zhang, "Estimation of inductance derivative for force control of linear switched reluctance actuator," *IEEE Transactions on Magnetics*, vol. 50, pp. 1-4, 2014.

[8] A. Labak and N. C. Kar, "Design and prototyping a novel 5-phase pancake shaped axial flux SRM for electric vehicle application through dynamic FEA incorporating flux-tube modeling," *IEEE Transactions on Industry Applications*, vol. 49, pp. 1276-1288, 2013.

[9] R. Madhavan and B. G. Fernandes, "Axial flux segmented SRM with a higher number of rotor segments for electric vehicles," *IEEE Transactions on Energy Conversion*, vol. 28, pp. 203-213, 2013.

[10] T. Yano, *Actuator with Multi Degrees of Freedom*, in Next-Generation Actuators Leading Breakthroughs, ed: Springer, pp. 279-290, 2010.

[11] G. Krebs, A. Tounzi, B. Pauwels, D. Willemot, and F. Piriou, "Modeling of a linear and rotary permanent magnet actuator," *IEEE Transactions on Magnetics*, vol. 44, pp. 4357-4360, 2008.

[12] M. Bertoluzzo, P. Bolognesi, O. Bruno, G. Buja, S. Castellan, V. Isastia, et al., "A distributed driving and steering system for electric vehicles using rotary-linear motors," in *Power Electronics Electrical Drives Automation and Motion, 2010 International Symposium on*, pp. 1156-1159, 2010.

[13] K. Meessen, J. Paulides, and E. Lomonova, "Analysis of a novel magnetization pattern for 2-DoF rotary-linear actuators," *IEEE Transactions on Magnetics*, vol. 48, pp. 3867-3870, 2012.

[14] Y. Sato, "Development of a 2-degree-of-freedom rotational/linear switched reluctance motor," *IEEE Transactions on Magnetics*, vol. 43, pp. 2564-2566, 2007.

[15] J. Pan, F. Meng, and G. Cao, "Decoupled control for integrated rotary–linear switched reluctance motor," *Electric Power Applications, IET*, vol. 8, pp. 199-208, 2014.

[16] J. F. Pan, Z. Yu, and N. C. Cheung, "Performance analysis and decoupling control of an integrated rotary-linear machine with coupled magnetic paths," *IEEE Transactions on Magnetics*, vol. 50, pp. 761-764, 2014.

[17] J. Pan, N. Cheung, and G.-Z. Cao, "Investigation of a rotary-linear switched reluctance motor," *XIX International Conference on Electrical Machines*, pp. 1-4, 2010.

[18] I. Bentia, L. Szabo, and M. Ruba, "On a rotary-linear switched reluctance motor," in *Power Electronics, Electrical Drives, International Symposium on Automation and Motion*, pp. 507-510, 2012.

[19] J. Cao, "A rotary-linear switched reluctance motor," in *2009 3rd International Conference on Power Electronics Systems and Applications*, pp. 1-4, 2009.

[20] *Slide Rotary Bush*. Available: http://www.nb-linear.co.jp/english/product/lineup/strokebush/sre.

html/, June 2015.

[21] J. Chang, D. Kang, I.-A. Viorel, and S. Larisa, "Transverse flux reluctance linear motor's analytical model based on finite-element method analysis results," *IEEE Transactions on Magnetics*, vol. 43, pp. 1201-1204, 2007.

[22] *Magnet CAD Package User Manual*, Infolytica Corporation Ltd., Montreal, Canada, 2007.